

This is the accepted manuscript made available via CHORUS. The article has been published as:

Angle-resolved photoemission spectroscopy view on the
nature of Ce

f electrons in the antiferromagnetic
Kondo lattice

CePd_5Al_2

Ya-Hua Yuan, Yu-Xia Duan, Ján Ruzs, Chen Zhang, Jiao-Jiao Song, Qi-Yi Wu, Yasmine Sassa, Oscar Tjernberg, Martin Månsson, Magnus H. Berntsen, Fan-Ying Wu, Shu-Yu Liu, Hao Liu, Shuang-Xing Zhu, Zi-Teng Liu, Yin-Zou Zhao, P. H. Tobash, Eric D. Bauer, Joe D. Thompson, Peter M. Oppeneer, Tomasz Durakiewicz, and Jian-Qiao Meng

Phys. Rev. B **103**, 125122 — Published 11 March 2021

DOI: [10.1103/PhysRevB.103.125122](https://doi.org/10.1103/PhysRevB.103.125122)

Angle-resolved photoemission spectroscopy view on the nature of Ce 4*f*-electrons in the antiferromagnetic Kondo lattice CePd₅Al₂

Ya-Hua Yuan,^{1,*} Yu-Xia Duan,^{1,*} Ján Ruzs,² Chen Zhang,¹ Jiao-Jiao Song,¹ Qi-Yi Wu,¹ Yasmine Sassa,^{2,3} Oscar Tjernberg,⁴ Martin Månsson,⁴ Magnus H. Berntsen,⁴ Fan-Ying Wu,¹ Shu-Yu Liu,¹ Hao Liu,¹ Shuang-Xing Zhu,¹ Zi-Teng Liu,¹ Yin-Zou Zhao,¹ P. H. Tobash,⁵ Eric D. Bauer,⁵ Joe D. Thompson,⁵ Peter M. Oppeneer,² Tomasz Durakiewicz,⁶ and Jian-Qiao Meng^{1,†}

¹*School of Physics and Electronics, Central South University, Changsha 410083, Hunan, People's Republic of China*

²*Department of Physics and Astronomy, Uppsala University, Box 516, S-75120 Uppsala, Sweden*

³*Department of Physics, Chalmers University of Technology, S-41296 Göteborg, Sweden*

⁴*Department of Applied Physics, KTH Royal Institute of Technology, Electrum 229, S-16440, Stockholm, Kista, Sweden*

⁵*Los Alamos National Laboratory, Los Alamos, New Mexico 87545, USA*

⁶*Institute of Physics, Maria Curie Skłodowska University, 20-031 Lublin, Poland*

(Dated: Wednesday 3rd February, 2021)

We report an angle-resolved photoemission spectroscopy study of the antiferromagnetic Kondo lattice CePd₅Al₂, focusing on the quasi-two-dimensional *k*-space nature of its Fermi surface and, tuning photon energy to the Ce 4*d*-4*f* on-resonance transition, the hybridization of the Ce 4*f* state. A strong shoulder feature on the *f*⁰ peak was detected, suggesting hybridization between conduction and *f* bands. On-resonance spectra revealed narrow, yet hybridized quasiparticle bands with sharp peaks and ~ 9 meV energy dispersion near the Fermi energy, E_F . The observed dispersive hybridized *f* band can be well described by a hybridization-band picture based on the periodic Anderson model. Hence, the 4*f* electrons in CePd₅Al₂ display a dual nature, with both localized and itinerant features, but with dominantly localized character.

PACS numbers: 74.25.Jb, 71.18.+y, 74.70.Tx, 79.60.-i

Heavy fermion (HF) compounds have been studied extensively for their rich physical properties since being discovered in 1975 [1]. Hybridization between itinerant conduction band electrons and localized *f*-electrons (*c*-*f*) plays a key role for several unique quantum states and quantum phase transitions, including: unconventional superconductivity [2], quantum criticality [3], antiferromagnetism [4], non-Fermi Liquid [5], possible Weyl fermion [6, 7], and topological nodal-line semimetal [8]. Many isostructural compounds RPd_5Al_2 ($R = \text{U, Ce, Y, Pr, Nd, Sm, Gd}$) have been successfully synthesized [9–13] since the neptunium-based HF superconductor $NpPd_5Al_2$ was first discovered in 2007 [9]. This series of HF compounds have a common tetragonal $ZrNi_2Al_5$ -type structure with the space group $I4/mmm$, in which the RPd_3 and Pd_2Al_2 layers are stacked along its *c*-axis. Several studies suggest that, except for the Y, Pr, and U compounds [10] most of the family members undergo antiferromagnetic (AFM) phase transitions at low temperature [9–13]. $PrPd_5Al_2$ compounds has a singlet ground states [11], and UPd_5Al_2 is a paramagnet [10].

CePd₅Al₂ has lattice parameters: $a = 4.156 \text{ \AA}$, $c = 14.883 \text{ \AA}$. It undergoes two magnetic transitions at $T_{N1} = 3.9 \text{ K}$ (or 4.1 K) and $T_{N2} = 2.9 \text{ K}$ [12–15]. Unlike $NpPd_5Al_2$, which exhibits superconductivity near its AFM ordering ($T_c = 4.9 \text{ K}$) at ambient pressure [9], bulk superconductivity of CePd₅Al₂ was induced by pressurization in the region of 9–12 GPa wherein it reached a

maximum $T_c = 0.57 \text{ K}$ [13]. An intermediate Sommerfeld coefficient γ , $60 \text{ mJ}/(\text{mol K}^2)$ for polycrystal [12] or $18 \text{ mJ}/(\text{mol K}^2)$ for single crystal [16], was estimated by specific heat experiments. This is greater than that of uncorrelated metals [$\sim 10 \text{ mJ}/(\text{mol K}^2)$] and less than that of typical HF compounds [$\sim 400 \text{ mJ}/(\text{mol K}^2)$]. This suggests that CePd₅Al₂ cannot be considered as a conventional HF compound. Ce 4*f* electrons are considered to be localized due to the small Sommerfeld coefficient γ [16]. Specific heat experiments suggested that the Ce³⁺ ion crystalline electric field (CEF) ground state is a Kramers doublet of well-localized 4*f* electron [13, 16, 17]. Inelastic neutron scattering measurements on a powder sample showed CEF excitations at 21.3 and 22.4 meV [15]. Single-crystal neutron diffraction observed an in-plane modulated magnetic structure [$Q = (0.235, 0.235, 0)$] below T_{N1} [14, 15]. Resistivity measurements indicated the presence of Kondo lattice and Fermi-Liquid behavior [12].

The electronic structure of CePd₅Al₂ appears to have quasi-two-dimensional (2D) characteristics [13] due to its layered structure and large interlayer distance. This is unusual in HF materials. We present the first angle-resolved photoemission spectroscopy (ARPES) data on this compound, utilizing tunable photon energies with high energy and momentum resolution on high-quality single crystals of CePd₅Al₂. Varying systematically the photon energies, we mapped the three-dimensional

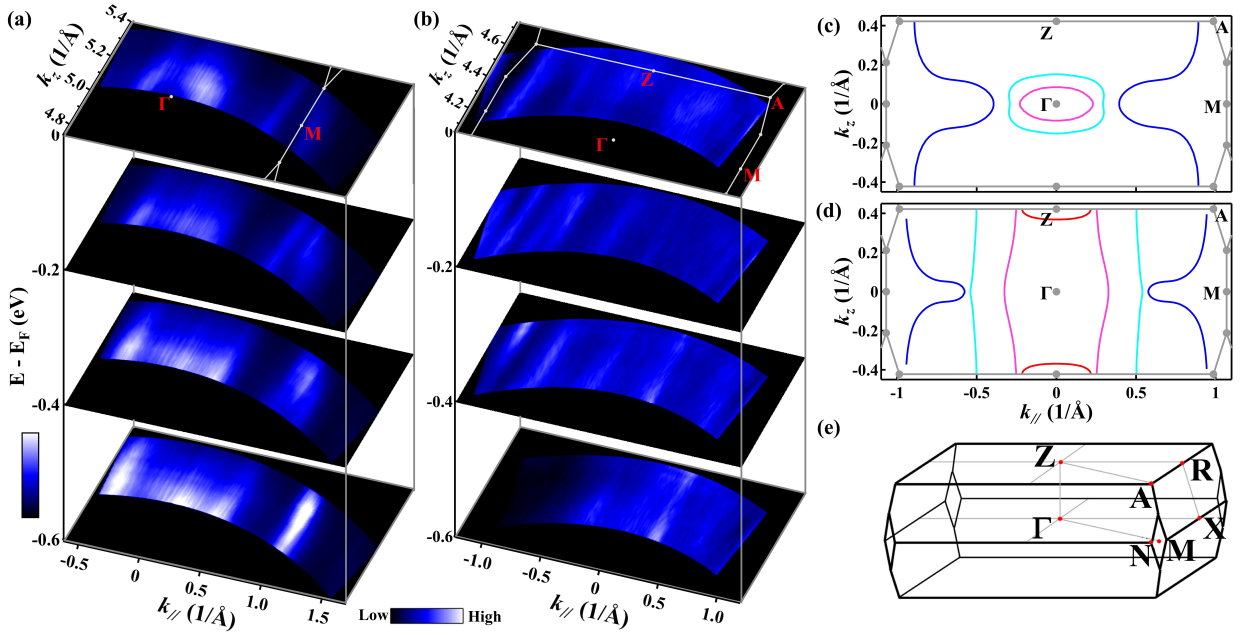


FIG. 1. (color online) (a) and (b) Experimental 3D FS maps constructed cuts along k_z in the Γ -M-A-Z plane and measured with $\hbar\nu = 87$ -100 and $\hbar\nu = 61$ -74 eV phonons, respectively. Band structure constant-energy contours are at E_F , and at 200, 400, and 600 meV below E_F , integrated over 20 meV. (c) and (d) DFT calculated Fermi contours in the Γ -M-A-Z plane for CePd₅Al₂ and LaPd₅Al₂, respectively. (e) The 3D Brillouin zone (BZ) of CePd₅Al₂ with high-symmetry momentum points marked.

Fermi surface (FS) of CePd₅Al₂ along the k_z (perpendicular) direction. The FS topology is compared to density-function theory (DFT) calculations. On-resonance $4d$ - $4f$ ARPES is measured to study the nature of Ce $4f$ -electrons.

Single crystals of CePd₅Al₂ were prepared by arc-melting stoichiometric amounts of the elements on a water-cooled copper hearth under a UHP argon atmosphere. The CePd₅Al₂ boule was crushed and small single crystals were extracted. ARPES measurements were carried out with VG-SCIENIA R4000 detectors at the SIS X09LA beamline of the Swiss Light Source. All samples were cleaved *in situ* along the (001) axis and measured in an ultrahigh vacuum with a base pressure better than 4×10^{-11} mbar. ARPES data were collected at $T = 10$ K, which is above the AFM transition temperature T_{N1} . An angular resolution of 0.2° was used for all measurements.

We used photon-energy dependent measurement to detect the k_z dispersion in the high-symmetry Γ -M-A-Z plane, to verify CePd₅Al₂ electronic structure dimensionality. The k_z dispersions are shown in Figs. 1(a) and (b), using a reasonable value for the inner potential V_0 of 16 eV. Data were collected using two different photon energy ranges 87-100 and 61-74 eV, covering half a BZ and including both Γ and Z points. The Fermi sheets show overall quasi-2D characters even though the shape and intensity of part of the Fermi sheets changed with photon energy (see Fig. S1 of the Supplemental Material [18] for

more details). The near E_F spectrum is greatly affected by the heavy f electron, which prevents clear FS detection. Weak k_z dispersion prevents an exact determination of the inner potential V_0 . Figs. 1(c) and (d) display the calculated FS topologies of CePd₅Al₂ and LaPd₅Al₂, respectively. The LaPd₅Al₂ band structure is calculated using the same lattice parameters as CePd₅Al₂, where only the $4f$ occupation is varied. LaPd₅Al₂ is a $4f^0$ rare-earth system with 3^+ valence. Itinerant and localized model calculations suggest different electronic structures along Γ -M. Both of these calculations are somewhat consistent with some of the experimental results, and some calculated dispersions were not observed in the data.

ARPES measurements were performed at the Ce $4d$ - $4f$ transition to enhance the f -electron spectral weight near E_F by tuning the photon energies to 123 eV. Fig. 2(a) shows the on-resonance spectra of CePd₅Al₂. Figs. 2(b) and 2(c) show the angle-resolved and angle-integrated photoemission spectroscopy of the intensity plot in (a), respectively. The high-intensity, dispersionless f^0 state is around -1.63 eV. This value is higher than that of other Ce-based HF compounds. For example, it is -2.5 eV for CePt₂In₇ [19], -2.3 eV for CeIrIn₅ [20], -2 eV for CeIn₃ [21], and -1.9 eV for CeRh₂Si₂ [22]. This flat band is generated by the pure charge excitations of the trivalent Ce ion ($4f^1 \rightarrow 4f^0$); it is commonly called the “ionization peak” [23]. In Figs. 2(a) and 2(b), slightly above the f^0 state, a weaker nondispersive structure was observed at around -1.3 eV. A shoulder appears at the

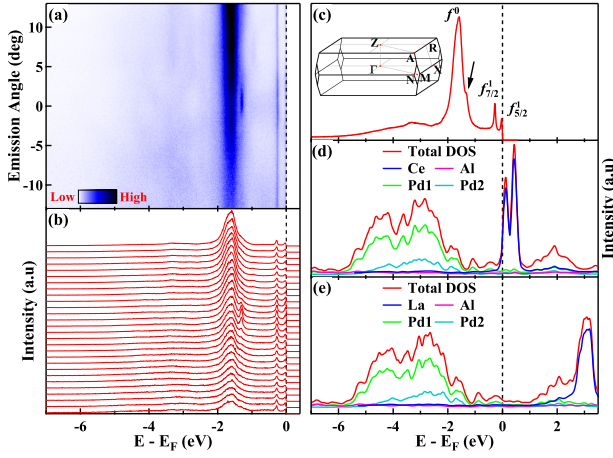


FIG. 2. (color online) (a) Raw data of a 2D image showing the on-resonance valence band structure for CePd_5Al_2 . The total energy resolution was set at ~ 30 meV. (b) Photoemission spectra (energy distribution curves, EDCs) corresponding to (a). (c) Angle-integrated photoemission spectroscopy of the intensity plot in (a). Inset: A 3D Brillouin zone with high-symmetry momentum points marked. Γ , M , N , and X are at the $k_z = 0$ plane while Z , A , and R points are at the $k_z = 2\pi/c$ plane. (d) Calculated Ce $4f$, Pd $3d$, and Al $3p$ density of state (DOS) vs. energy E for CePd_5Al_2 . (e) The calculated DOS of CePd_5Al_2 's isostructural compound LaPd_5Al_2 .

front edge of the huge f^0 peak. It is indicated by the arrow in Fig. 2(c). The calculation suggests that the valence band does not have a flat band around this energy. Such a shoulder of the f^0 peak probably originates from hybridization spreading [21, 22].

The Ce $4f$ character is strongly enhanced, as demonstrated by the heavy quasiparticle bands (f^1 state) close to E_F [Fig. 2(c)]. Spin-orbit splitting results in an f^1 state that splits into two sharp peaks, $f_{7/2}^1$ and $f_{5/2}^1$. The $f_{7/2}^1$ state is located at ~ 280 meV below E_F . The $f_{5/2}^1$ state is located near E_F . These characteristic features are widely founded in Ce-based HF compounds [19–26]. The $4f^1$ state intensity is much weaker than that of other itinerant f -electron HF compounds such as URu_2Si_2 [27, 28]. It is stronger than that of partially itinerant f -electron HF compounds such as CePt_2In_7 [19]. According to the single-impurity Anderson model (SIAM), it is widely accepted that the f^1 -to- f^0 intensity ratio, $[I(f_{7/2}^1) + I(f_{5/2}^1)]/I(f^0)$, can reflect the hybridization strength. The CePd_5Al_2 f^1 -to- f^0 intensity ratio is about 0.11 (See Fig. S2 of the Supplemental Material [18] for more details). It is stronger than that of CePt_2In_7 [19], and much weaker than that of CeMIn_5 [20, 24]. It can be deduced that CePd_5Al_2 hybridization strength is stronger than that of CePt_2In_7 and weaker than that of CeMIn_5 .

Fig. 2(d) and 2(e) display comparisons of the calculated DOS of the isostructural compounds CePd_5Al_2 and LaPd_5Al_2 , respectively. DFT calculations suggest that,

unlike LaPd_5Al_2 , where the La $4f$ electrons are well above E_F , the Ce $4f$ electrons in CePd_5Al_2 are mostly located just about 0.1 eV above E_F , and a small amount of Ce $4f$ electrons appears below E_F . The feature close to E_F is considered to originate from the tail of the Kondo resonance peak above E_F .

A comparison of spectra dominated by d -band spectral weight with spectra having Ce $4f$ weight resonantly enhanced provides insight in the basic localization or itinerant properties of the $4f$ electrons. The three spectra range from off- to on-resonance are shown in Fig. 3. Close to E_F , the off-resonance spectrum ($h\nu = 115$ eV) shows a density of states of non- f orbital character dominated by Pd $4d$ states [Fig. 3(a)]. The conduction band intensity is weak, possibly due to the emission from Pd $4d$ state which is strongly suppressed by the Cooper minimum around 115 eV [29]. Dominant Pd $4d$ emission in the off-resonance spectrum is replaced by the Ce $4f$ emission in the on-resonance spectrum as photon energy changes [Fig. 3(c)]. A Fano resonance enhancement of the Ce $4f$ emission at 123 eV photon energy reveals an on-resonance spectrum which shows a gathering of Ce $4f$ spectra weight near E_F . The intense $4f$ character near E_F is seen in the angle-integrated spectra (Fig. 3(d)). Two flat quasiparticle bands, $f_{7/2}^1$ and $f_{5/2}^1$ state, formed by spin-orbital splitting, appear just below E_F . The non-resonance spectrum can also distinguish two Kondo resonance peaks having very weak intensity. They originate from the Ce $4f$ electrons. The intensity of the two flat bands shows an obvious momentum dependence. Flat band spectral weight is markedly stronger around the f and conduction bands intersection than that of other positions. The $f_{5/2}^1$ state strength is much weaker than that of $f_{7/2}^1$ suggesting that hybridization is weaker [30].

When hybridization occurs, in addition to the redistribution of the f -electron spectrum weight, a dispersive heavy quasiparticle band should be observed around the intersection of the f band and conduction band. Thus, we measured high energy resolution on-resonance spectra were along the direction slightly deviating from Γ' - M' . The c - f hybridization feature is easily detected as shown by the dispersive heavy band near E_F , and the redistribution of the f -electron spectrum [Fig. 4(a)]. A fraction of the Ce $4f$ electrons are itinerant and involved in FS formation. Note that this is different from a transport measurement viewpoint [16]. Hybridization between $f_{5/2}^1$ and conduction electrons is a common feature in Ce-based HFs [19–22, 24, 25]. No discernible dispersion was observed for the $4f_{7/2}^1$ state. This may be due to insufficient energy and momentum resolution of the measurement, and that the intensity of the $4f_{7/2}^1$ state is much higher than that of the conduction band.

Fig. 4(b) shows the EDCs corresponding to Fig. 4(a). The heavy quasiparticle band peaks near the intersections, indicated by open circles, vary with momentum.

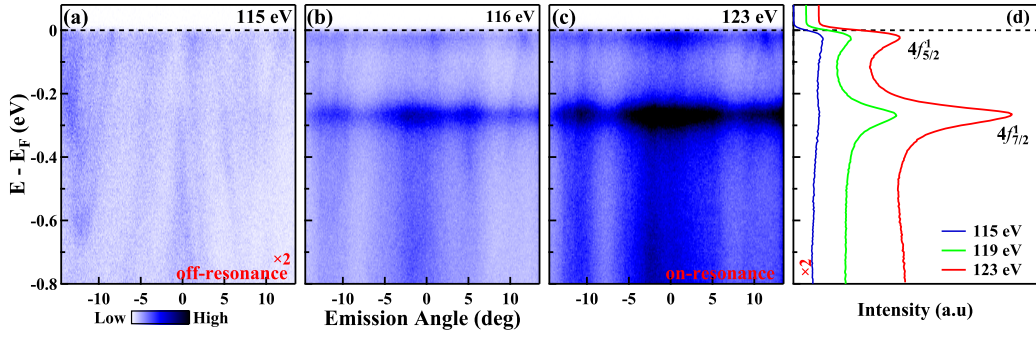


FIG. 3. (color online) (a)-(c) Raw band maps of CePd_5Al_2 along $\text{M}'\text{-}\Gamma\text{'-}\text{M}'$ directions taken at photon energies of 115, 119, and 123 eV, respectively. This set of data shows the evolution of momentum resolved Ce $4f$ emissions across the Ce $4d\text{-}4f$ threshold. (d) The angle-integrated EDCs for data in panels (a)-(c). The positions of the $f_{5/2}^1$ and $f_{7/2}^1$ states are indicated.

Fig. 4(c) shows the integrated EDCs at five selected momentum positions shown in different colors in Fig. 4(a). This includes the conduction bands that cross the E_F region and adjacent regions where no conduction bands cross the E_F . EDC peak positions in these two regions differ. EDC peak positions in the former regions shift ~ 9 meV towards high binding energy. This value is similar to that of CePt_2In_7 (5 meV) [19] and CeIn_3 (4 meV) [21],

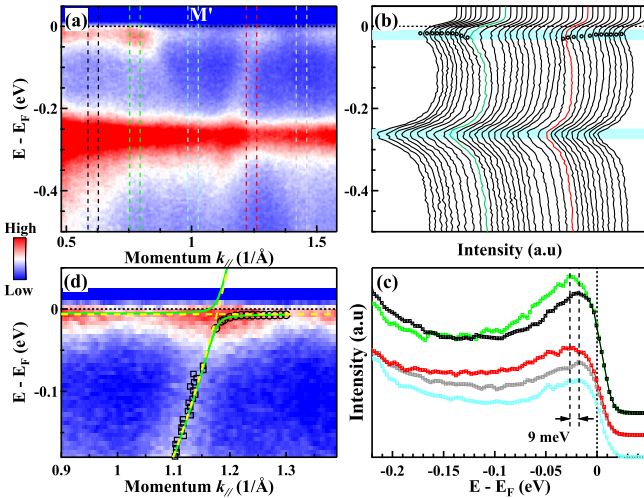


FIG. 4. (Color online) (a) On-resonance valence band structure of CePd_5Al_2 measured along a direction slightly off $\Gamma'\text{-}\text{M}'$. (b) EDCs of the spectra shown in (a). Aqua shadows indicate $f_{5/2}^1$ and $f_{7/2}^1$ states positions. The open circles indicate EDCs peak positions. (c,d) Comparison of EDCs measured at different momentum positions. The black, green, aqua, red, and grey curves were obtained by integrating the regions between two black, green, aqua, red, and grey dashed lines, as indicated in (a), respectively. (d) Photoemission intensity near the E_F . Squares and open circles represent the conduction and hybridized f bands position, respectively. The hybridized dispersion was fitted by the equation based on the periodic Anderson model, as indicated by green lines. The horizontal and parabolic yellow-dashed lines represent the f -level and bare conduction band, respectively.

but significantly smaller than that of CeIrIn_5 (about 30 meV)[33]. EDCs peak positions in non-intersecting regions are almost identical (black, aqua, and grey curves). The periodic Anderson model suggests that, the stronger the $c\text{-}f$ hybridization, the greater the energy shift in the f -level band. This means that the hybridization strength between f -band and conduction band of CePd_5Al_2 is obviously weaker than that of CeIrIn_5 .

Fig. 4(d) presents a zoomed view into the intersections of the f band and conduction band, and the data has been divided by the corresponding resolution-convoluted Fermi-Dirac function. A weak dispersionless band is observed between the f band and the conduction band intersection. This could be due to the strong Kondo resonance just below E_F . The conduction bands represented by the squares and the hybridized f band represented by the open circles were obtained by fitting momentum distribution curves (MDCs) and tracking energy distribution curves (EDCs) peak positions, respectively. According to previous work [20, 24, 30], although CePd_5Al_2 is not in a Fermi liquid state, its ARPES spectrum can still be analyzed according to the hybridization band picture based on the periodic Anderson model (PAM) [30, 31], in which the hybridization build upper (E^+) and lower (E^-) bands that are given by

$$E^\pm(k) = \frac{\varepsilon_0 + \varepsilon_k \pm \sqrt{(\varepsilon_0 - \varepsilon_k)^2 + 4|V_k|^2}}{2},$$

where ε_0 is the renormalized f -level energy ($\text{Ce } 4f_{5/2}^1$), ε_k is the bare conduction band, and V_k is the renormalized hybridization (half of the direct hybridization gap) [30]. A good fit result (solid green lines) is achieved [Fig. 4(d)]. This is accomplished by fitting, $\varepsilon_0 = -6.2$ meV, and $V_k = 16 \pm 2$ meV. This corresponds to a direct hybridization gap of ~ 32 meV. This value is similar to that of 30 meV in CeCoIn_5 [24] and 36 meV in CeIrIn_5 [20]. The indirect gap, obtained by a previous theory calculation, is $\Delta_g \sim 2V_k^2/D$, where D ($D \gg \varepsilon_0$) is the half-bandwidth of the bare conduction band, and thus vanishingly small. The fitted results show that the energy spacing between the

bottom of the E^+ band and the top of the E^- band is quite small. The obtained negative ε_0 value, similar to that of γ -Ce [32], indicates a ground state f -level of CePd_5Al_2 has a position just several meV below E_F .

To conclude, we investigated the 3D FS topology and the properties of f -electrons in the antiferromagnetic Kondo lattice CePd_5Al_2 at low temperatures using high-resolution ARPES. A quasi-2D nature of FSs was detected. Heavy $4f$ -derived sharp quasiparticle bands, a strong and sharp $4f^0$ peak at -1.63 eV below E_F , and spin-orbit splitting of the $4f^1$ final state into $f_{7/2}^1$ and $f_{5/2}^1$ final states were directly observed. Furthermore, a shoulder of the f^0 peak, a redistribution of f^1 electrons, and a weak dispersive heavy quasiparticle band with an energy shift of ~ 9 meV just below the E_F were observed. The sharp heavy quasiparticle peaks ($f_{5/2}^1$ and $f_{7/2}^1$) near E_F and the hybridized f band indicate that the f electrons are partially itinerant at low temperature, yet dominantly localized. This dual nature of the $4f$ state is derived here from its small but detectable hybridization in CePd_5Al_2 .

This work was supported by the National Natural Science Foundation of China (Grant No. 12074436, 11574402), and the Innovation-driven Plan in Central South University (Grant No. 2016CXS032). J.R. and P.M.O. acknowledge support through the Swedish Research Council (VR) and the Swedish National Infrastructure for Computing (SNIC), for computing time on computer cluster Triolith at the NSC center Linköping. Y.S. acknowledges the support from the Swedish Research Council (VR) through a Starting Grant (Dnr. 2017-05078). O.T. acknowledges support from the Swedish Research Council (VR) and the Knut and Alice Wallenberg foundation. M.M. is partly supported by a Marie Skłodowska-Curie Action, International Career Grant through the European Commission and Swedish Research Council (VR), Grant No. INCA-2014-6426, as well as a VR neutron project grant (BIFROST, Dnr. 2016-06955). Further support was also granted by the Carl Tryggers Foundation for Scientific Research (Grant No. CTS-16:324 and No. CTS-17:325). Work at Los Alamos was performed under the auspices of the U.S. Department of Energy, Office of Basic Energy Sciences, Division of Materials Sciences and Engineering.

* These two authors contributed equally

† Corresponding author: jqmeng@csu.edu.cn

- [1] K. Andres, J. Graebner, and H. Ott, Phys. Rev. Lett. **351**, 1779 (1975).
- [2] F. Steglich, J. Aarts, C. D. Bredl, W. Lieke, D. Meschede, W. Franz, and H. Schäfer, Phys. Rev. Lett. **43**, 1892 (1979).
- [3] P. Gegenwart, Q. Si, and F. Steglich, Nature Physics **4**, 186 (2008).
- [4] N. apRoberts-Warren, A. P. Dioguardi, A. C. Shockley, C. H. Lin, J. Crocker, P. Klavins, and N. J. Curro, Phys. Rev. B **81**, 180403(R) (2010).
- [5] V. A. Sidorov, M. Nicklas, P. G. Pagliuso, J. L. Sarrao, Y. Bang, A. V. Balatsky, and J. D. Thompson, Phys. Rev. Lett. **89**, 157004 (2002).
- [6] Y. Xu, C. Yue, H. Weng, and X. Dai, Phys. Rev. X **7**, 11027 (2017).
- [7] C. Y. Guo, F. Wu, Z. Z. Wu, M. Smidman, C. Cao, A. Bostwick, C. Jozwiak, E. Rotenberg, Y. Liu, F. Steglich, and H. Q. Yuan, Nat. Commun. **9**, 4622 (2018).
- [8] C. Cao, G. X. Zhi, and J. X. Zhu, Phys. Rev. Lett. **124**, 166403 (2020).
- [9] D. Aoki, Y. Haga, T. D. Matsuda, N. Tateiwa, S. Ikeda, Y. Homma, H. Sakai, Y. Shiokawa, E. Yamamoto, A. Nakamura, R. Settai, and Y. Ōnuki, J. Phys. Soc. Jpn. **76**, 063701(2007).
- [10] Y. Haga, D. Aoki, Y. Homma, S. Ikeda, T. D. Matsuda, E. Yamamoto, H. Sakai, N. Tateiwa, N. D. Dung, A. Nakamura, Y. Shiokawa, and Y. Ōnuki, J. Alloys Compd. **464**, 47 (2008).
- [11] R. A. Ribeiro, Y. F. Inoue, T. Onimaru, M. A. Avila, K. Shigetoh, and T. Takabatake, Physica B: Condensed Matter **404**, 2946 (2009).
- [12] R. A. Ribeiro, T. Onimaru, K. Umeo, M. de Abreu Avila, K. Shigetoh, and T. Takabatake, J. Phys. Soc. Jpn. **76**, 123710 (2007).
- [13] F. Honda, M.A. Measson, Y. Nakano, N. Yoshitani, E. Yamamoto, Y. Haga, T. Takeuchi, H. Yamagami, K. Shimizu, R. Settai, and Y. Ōnuki, J. Phys. Soc. Jpn. **77**, 43701 (2008).
- [14] Y. F. Inoue, T. Onimaru, A. Ishida, T. Takabatake, Y. Oohara, T. J. Sato, D. T. Adroja, A. D. Hillier, and E. A. Goremychkin, Journal of Physics: Conference Series **200**, 32023 (2010).
- [15] T. Onimaru, Y. F. Inoue, A. Ishida, K. Umeo, Y. Oohara, T. J. Sato, D. T. Adroja, and T. Takabatake, Journal of Physics: Condensed Matter **31**, 125603 (2019).
- [16] T. Onimaru, Y. F. Inoue, K. Shigetoh, K. Umeo, H. Kubo, R. A. Ribeiro, A. Ishida, M. A. Avila, K. Ohoyama, M. Sera, and T. Takabatake, J. Phys. Soc. Jpn. **77**, 074708 (2008).
- [17] Y. Nakano, F. Honda, T. Takeuchi, K. Sugiyama, M. Hagiwara, K. Kindo, E. Yamamoto, Y. Haga, R. Settai, H. Yamagami, and Y. Ōnuki, J. Phys. Soc. Jpn. **79**, 024702(2010).
- [18] See Supplemental Material for Band structures of CePd_5Al_2 with different photon energies, and calculation of f^1 -to- f^0 ratio.
- [19] Y. X. Duan, C. Zhang, J. Rusz, P. M. Oppeneer, T. Durakiewicz, Y. Sassa, O. Tjernberg, M. Månsson, M. H. Berntsen, F.Y. Wu, Y.Z. Zhao, J.J. Song, Q.Y. Wu, Y. Luo, E. D. Bauer, J. D. Thompson, and J. Q. Meng, Phys. Rev. B **100**, 085141 (2019).
- [20] Q. Y. Chen, C. H. P. Wen, Q. Yao, K. Huang, Z. F. Ding, L. Shu, X. H. Niu, Y. Zhang, X. C. Lai, Y. B. Huang, G. B. Zhang, S. Kirchner, and D. L. Feng, Phys. Rev. B **97**, 075149(2018).
- [21] Yun Zhang, Wei Feng, Xia Lou, Tianlun Yu, Xiegang Zhu, Shiyong Tan, Bingkai Yuan, Yi Liu, Haiyan Lu, Donghua Xie, Qin Liu, Wen Zhang, Xuebing Luo, Yaobo Huang, Lizhu Luo, Zhengjun Zhang, Xinchun Lai, and Qiuyun Chen, Phys. Rev. B **97**, 045128 (2018).
- [22] S. Patil, A. Generalov, M. Güttler, P. Kushwaha, A.

- Chikina, K. Kummer, T. C. Rödel, A. F. Santander-Syro, N. Caroca-Canales, C. Geibel, S. Danzenbächer, Yu. Kucherenko, C. Laubschat, J. W. Allen, and D. V. Vyalikh, *Nat. Commun.* **7**, 11029 (2016).
- [23] J. W. Allen, S. J. Oh, O. Gunnarsson, K. Schönhammer, M. B. Maple, M. S. Torikachvili, and I. Lindau, *Adv. Phys.* **35**, 275-316 (1986).
- [24] Q. Y. Chen, D. F. Xu, X. H. Niu, J. Jiang, R. Peng, H. C. Xu, C. H. P. Wen, Z. F. Ding, K. Huang, L. Shu, Y. J. Zhang, H. Lee, V. N. Strocov, M. Shi, F. Bisti, T. Schmitt, Y. B. Huang, P. Dudin, X. C. Lai, S. Kirchner, H. Q. Yuan, and D. L. Feng, *Phys. Rev. B* **96**, 045107 (2017).
- [25] H. Liu, Y. Xu, Y. Zhong, J. Guan, L. Kong, J. Ma, Y. Huang, Q. Chen, G. Chen, M. Shi, Y. Yang, and H. Ding, *Chinese Physics Letters* **36**, 097101(2019).
- [26] Y. Luo, C. Zhang, Q. Y. Wu, F. Y. Wu, J. J. Song, W. Xia, Y. F. Guo, J. Ruzs, P. M. Oppeneer, T. Durakiewicz, Y. Z. Zhao, H. Liu, S. X. Zhu, Y. H. Yuan, X. F. Tang, J. He, S. Y. Tan, Y. B. Huang, Z. Sun, Y. Liu, H. Y. Liu, Y. X. Duan, and J. Q. Meng, *Phys. Rev. B* **101**, 115129 (2020).
- [27] S.-I. Fujimori, Y. Saitoh, T. Okane, A. Fujimori, H. Yamagami, Y. Haga, E. Yamamoto, and Y. Onuki, *Nature Physics* **3**, 618(2007).
- [28] J. Q. Meng, P. M. Oppeneer, J. A. Mydosh, P. S. Riseborough, K. Gofryk, J. J. Joyce, E. D. Bauer, Y. Li, and T. Durakiewicz, *Phys. Rev. Lett* **111**, 127002 (2013).
- [29] J. J. Yeh and I. Lindau, *At. Data Nucl. Data Tables* **32**, 1(1985).
- [30] H. J. Im, T. Ito, H. D. Kim, S. Kimura, K. E. Lee, J. B. Hong, Y. S. Kwon, A. Yasui, and H. Yamagami, *Phys. Rev. Lett.* **100**, 176402 (2008).
- [31] P. Coleman, (2015). Heavy electrons. In *Introduction to Many-Body Physics* (pp. 656-719). Cambridge: Cambridge University Press.
- [32] X. Zhu, Y. Liu, Y. Zhao, Y. Wang, Y. Zhang, C. Lu, Y. Duan, D. Xie, W. Feng, D. Jian, Y. Wang, S. Tan, Q. Liu, W. Zhang, Y. Liu, L. Luo, X. Luo, Q. Chen, H. Song, and X. Lai, *npj Quantum Materials* **5**, 47(2020).
- [33] S. I. Fujimori, A. Fujimori, K. Shimada, T. Narimura, K. Kobayashi, H. Namatame, M. Taniguchi, H. Harima, H. Shishido, S. Ikeda, D. Aoki, Y. Tokiwa, Y. Haga, and Y. Onuki, *Phys. Rev. B* **73**, 224517 (2006).